THE JOURNAL OF BIOLOGICAL CHEMISTRY
Vol. 279, No. 27, Issue of July 2, pp. 28689–28696, 2004
Printed in U.S.A.

Structural Insights into Endosomal Sorting Complex Required for Transport (ESCRT-I) Recognition of Ubiquitinated Proteins*

Received for publication, January 5, 2004, and in revised form, March 22, 2004
Published, JBC Papers in Press, March 24, 2004, DOI 10.1074/jbc.M400023200

Hsiangling Teo‡§, Dmitry B. Veprintsev¶, and Roger L. Williams‡‖

From the ‡Medical Research Council Laboratory of Molecular Biology and ¶Centre for Protein Engineering, Medical Research Council Centre, Cambridge CB2 2QH, United Kingdom

The endosomal sorting complex required for transport (ESCRT-I) is a 350-kDa complex of three proteins, Vps23, Vps28, and Vps37. The N-terminal ubiquitin-conjugating enzyme E2 variant (UEV) domain of Vps23 is required for sorting ubiquitinated proteins into the internal vesicles of multivesicular bodies. UEVs are homologous to E2 ubiquitin ligases but lack the conserved cysteine residue required for catalytic activity. The crystal structure of the yeast Vps23 UEV in a complex with ubiquitin (Ub) shows the detailed interactions made with the bound Ub. Compared with the solution structure of the Tsg101 UEV (the human homologue of Vps23) in the absence of Ub, two loops that are conserved among the ESCRT-I UEVs move toward each other to grip the Ub in a pincer-like grasp. The contacts with the UEV encompass two adjacent patches on the surface of the Ub, one containing several hydrophobic residues, including Ile-8$_{Ub}$, Ile-44$_{Ub}$, and Val-70$_{Ub}$, and the second containing a hydrophilic patch including residues Asn-60$_{Ub}$, Gln-62$_{Ub}$, Glu-64$_{Ub}$. The hydrophobic Ub patch interacting with the Vps23 UEV overlaps the surface of Ub interacting with the Vps27 ubiquitin-interacting motif, suggesting a sequential model for ubiquitinated cargo binding by these proteins. In contrast, the hydrophilic patch encompasses residues uniquely interacting with the ESCRT-I UEV. The structure provides a detailed framework for design of mutants that can specifically affect ESCRT-I-dependent sorting of ubiquitinated cargo without affecting Vps27-mediated delivery of cargo to endosomes.

Ubiquitination serves as a general mechanism for regulating protein localization and destiny in eukaryotic cells. This mechanism involves conjugation of the 76-residue polypeptide ubiquitin (Ub)[1] to the ϵ-amino group of lysine residues on target proteins. The conjugation occurs by means of a sequential series of thiolester-bound intermediates involving the E1, E2, and E3 enzymes and results in proteasomal, nuclear, and endosomal targeting, depending upon the protein and the nature of the ubiquitination. Whereas proteasomal targeting requires attachment of a chain of at least four ubiquitins linked by isopeptide bonds between the C terminus of one Ub and Lys-48 of the next (1, 2), mono-ubiquitination is sufficient for endosomal targeting. Ubiquitination regulates internalization and/or MVB sorting of many transmembrane proteins, such as receptor tyrosine kinases (RTKs), G-protein coupled receptors, ion channels, transporters, and permeases (reviewed in Refs. 3–6). Ub-mediated endocytosis of RTKs is a principle mechanism for their down-regulation (7). Although mono-ubiquitination of RTKs is sufficient for endocytosis, several RTKs are mono-ubiquitinated at multiple sites (8, 9), potentially changing the dynamics of endocytosis. For yeast uracil permease, mono-ubiquitination is sufficient for endocytosis, but Lys-63-linked polyubiquitination seems to stimulate the process (10).

The role of ubiquitination in endocytosis is not limited to initial internalization of proteins from the plasma membrane. Once proteins are localized to endosomal membranes, ubiquitination serves to sort proteins into internal vesicles within the endosomes through inward budding-forming structures known as multivesicular bodies (MVBs). The late endosomes containing MVBs eventually fuse with lysosomes to degrade the internal vesicles and their protein cargo (11).

In yeast, sorting into MVBs involves the endosomal-sorting complex required for transport (ESCRT-I). This 350-kDa complex is made up of three proteins, Vps23, Vps28, and Vps37 (12, 13). The mammalian homologue of Vps23, the tumor susceptibility gene (Tsg101), is also part of a 350-kDa complex that binds Ub and mediates the sorting of ubiquitinated proteins into vesicles (13, 14); however, the mammalian homologue of Vps37 has not yet been identified. Both Vps23 and Tsg101 have an N-terminal domain known as a Ub-conjugating enzyme E2 variant (UEV) (15, 16). UEVs are homologous to E2 ligases but lack a cysteine necessary for catalysis (17). Compared with the E2 ligases, the UEVs form only a small family of proteins, with only a few representatives in the human genome (Figs. 1 and 2). One of the genes (UEV-1 or Croc-1) encodes several splice variants. The UEVs constitute an ancient protein family with a conserved structure, which is related to but distinct from the E2 ligases (15, 16, 18). The first characterized UEVs, UEV-1A (Croc-1A) and Mms2, form complexes with the E2 ligase Ubc13, which function with the E3 ring proteins TRAF6 and Rad6, respectively, to catalyze the assembly of Lys-63-linked polyubiquitin chains (19–21). UEVs can occur as single-domain proteins, as in the case of Mms2, or within multi-domain proteins, such as the human UEV-1B and UEV3, which are fused to fatty-acid hydrolase (22) and lactate dehydrogenase domains (23), respectively. Vps23 homologues having an N-terminal

* The costs of publication of this article were defrayed in part by the payment of page charges. This article must therefore be hereby marked "*advertisement*" in accordance with 18 U.S.C. Section 1734 solely to indicate this fact.

The atomic coordinates and structure factors (code 1uzx) have been deposited in the Protein Data Bank, Research Collaboratory for Structural Bioinformatics, Rutgers University, New Brunswick, NJ (http://www.rcsb.org/).

§ Supported by the Agency for Science, Technology and Research of Singapore.

‖ To whom correspondence should be addressed. Tel.: 44-1223-402171; Fax: 44-1223-412178; E-mail: rlw@mrc-lmb.cam.ac.uk.

[1] The abbreviations used are: Ub, ubiquitin; RTK, receptor tyrosine kinases; MVB, multivesicular bodies; ESCRT, endosomal sorting complex required for transport; Vps, vacuolar protein sorting; Tsg, tumor susceptibility gene; UEV, ubiquitin-conjugating enzyme E2 variant; MAD, multiple anomalous dispersion; CCD, charge-coupled device; ESRF, European Synchrotron Radiation Facility; SAD, single anomalous dispersion; UIM, ubiquitin-interacting motif; UBC, Ub-conjugating enzyme.

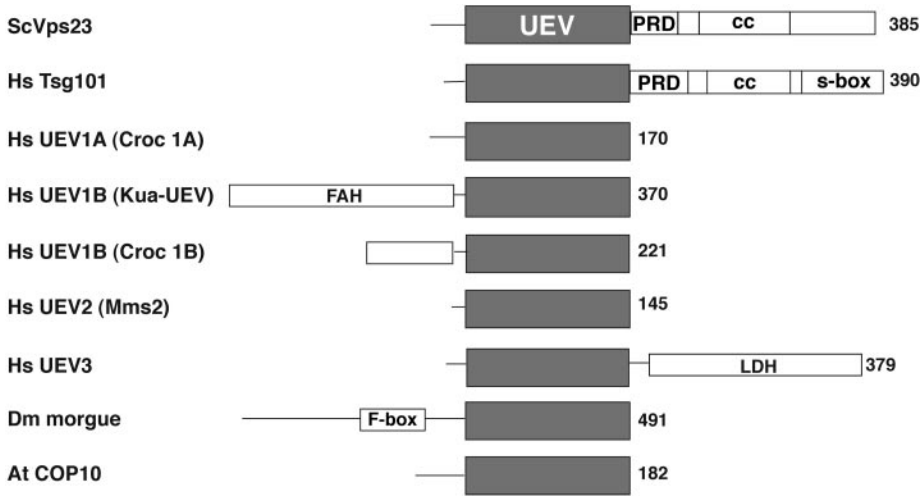

FIG. 1. **A schematic illustration of the domain organization of UEV-containing proteins.** *FAH*, fatty-acid hydrolase; *LDH*, lactate dehydrogenase; *PRD*, proline-rich domain; *CC*, coiled-coil region; *s-box*, "steadiness" box (67). Species abbreviations are: *Sc*, *Saccharomyces cerevisiae*; *Hs*, human; *Dm*, *Drosophila melanogaster*; and *At*, *Arabidopsis thaliana*.

UEV domain are conserved in eukaryotes from yeasts to mammals. The UEV domain of Vps23/Tsg101 is necessary for the sorting of ubiquitinated cargo to MVBs (12, 24) and for viral budding in mammalian cells (25–27).

In addition to binding ubiquitinated cargo, the Vps23 UEV domain interacts with Vps27, the yeast homologue of the mammalian Hrs, by means of PTVP and PSDP motifs in the Vps27, and this interaction recruits ESCRT-I to endosomal membranes (28, 29). The PTVP and PSDP motifs of Vps27 are analogous to a PSAP motif in Hrs that interacts with the Tsg101 UEV domain (30–32). The Tsg101 UEV domain is also able to recognize a PTAP motif from the late domain p6 protein of HIV-1 Gag, and this PTAP binding is necessary for efficient viral budding (25, 26). The interaction between the Tsg101 UEV and the HIV-1 p6 protein seems to recruit the ESCRT complexes to the plasma membrane in a manner that mimics the recruitment of the ESCRT complexes to the early endosomes (reviewed in Rev. 33).

The UEVs are members of a set of structurally unrelated protein modules capable of specifically recognizing ubiquitinated proteins. Several modules, such as the UIM, UBA, CUE, and NZF domains, have been characterized recently (34–42). In most cases, the molecular details of the Ub/recognition module interaction have been indirectly inferred from site-specific mutagenesis or from NMR chemical shift changes in the recognition modules elicited by the addition of Ub. Two notable exceptions are the structures of CUE domain/Ub complexes (35, 36) and the structure of the Vps27 UIM domain/Ub complex (43). We report here the 1.85 Å resolution x-ray crystal structure of the Vps23 UEV domain in a complex with Ub.

EXPERIMENTAL PROCEDURES

Plasmids—The sequence encoding the UEV domain of *S. cerevisiae* Vps23 (residues 1–161) was cloned into vector pOPCH using NdeI-BamHI sites, resulting in a construct with an MAH_6 affinity tag immediately preceding residue Met-1. The construct was verified by sequencing.

Protein Expression and Purification—Selenomethionine-substituted protein was grown in methionine-requiring B834 (DE3) cells in M9 minimal media supplemented with 1 mg/l riboflavin, 1 mg/liter niacinamide, 1 mg/liter pyridoxine monohydrochloride, 1 mg/liter thiamine, 0.4% D(+)-glucose, 2 mM $MgSO_4$, 25 mg/liter $FeSO_4$, 40 mg/liter of each amino acids except methionine, 40 mg/liter seleno-L-methionine, and 0.1 g/liter ampicillin. Cells were grown at 37 °C to A_{600} = 1.0, then induced with 0.3 mM isopropyl-1-thio-β-D-galactopyranoside and incubated at 16 °C for 12 h. Native protein was expressed in C41(DE3) cells.

Cells were resuspended in buffer A (20 mM Tris, pH 8.0, 50 mM potassium phosphate, pH 8.0, and 100 mM NaCl) and disrupted with a French press. After ultracentrifugation, the supernatant was loaded onto a Ni^{2+}-affinity column equilibrated with buffer B (Buffer A + 15 mM imidazole) and eluted with an imidazole gradient. Fractions containing Vps23 UEV were pooled and diluted with an equal volume of buffer C (20 mM Tris, pH 8.0, 2 mM dithiothreitol), loaded onto a Q-Sepharose column, and eluted with a NaCl gradient. Fractions containing Vps23 UEV were pooled, concentrated, and purified by gel filtration on Superdex 75 16/60 equilibrated in buffer D (20 mM Tris, pH 7.4, 100 mM NaCl, and 5 mM dithiothreitol). The purified Vps23 UEV domain was concentrated to 78 mg/ml for crystallization screens.

Analytical Ultracentrifugation—Sedimentation equilibrium experiments were done in a Beckman Optima XLI analytical ultracentrifuge with Ti-60 rotor using interference and absorbance at 280 and 230 nm, at 10 °C. The Vps23 UEV in 10 mM Hepes, pH 7.4, 50 mM NaCl was loaded into six-sector 12-mm path length cells at three different concentrations: 3, 18, and 470 μM. The samples were spun at 22,000, 28,000 and 35,000 rpm until they reached equilibrium, as judged by the changes in the subsequent scans. Data were analyzed using UltraSpin software (available on the World Wide Web at www.mrc-cpe.cam.ac.uk). The Vps23 UEV was monomeric at loading concentrations of 3 and 18 μM. At the highest concentration used (470 μM), higher order oligomers of ~90,000 ± 10,000 were detected. The relative proportion of the oligomeric species decreased as the speed increased, suggesting that it was removed from the equilibrium, possibly by forming large oligomers that sedimented to the bottom of the cell.

Crystallization—Solutions for 1200 crystallization conditions were dispensed into reservoirs of 96-well crystallization plates (Corning, NY). Protein (100 nl) and reservoir (100 nl) solutions were added to the plates as sitting drops using a Cartesian robot (Genomics Solutions, Huntingdon, UK) and incubated at 17 °C. The selenomethionine-substituted Vps23 UEV domain was mixed with bovine Ub (Sigma) at a 1:1.1 molar ratio. Optimal crystals were obtained in 22% polyethylene glycol 8000, 0.1 M 4-morpholineethanesulfonic acid, pH 6.5, and 0.2 M $(NH_4)_2SO_4$. Crystals used for data collection were grown by hair seeding in hanging drops containing 0.5 μl of protein mixed with 0.5 μl of reservoir solution. Crystals were cryoprotected by incubation over a reservoir containing mother liquor supplemented with 35% polyethylene glycol 8000 for at least 48 h; they were then frozen in a cryostream at 100 K.

Data Collection, Phasing, and Model Refinement—Data were collected at 100 K from crystals frozen in a nitrogen gas stream. Multiple anomalous dispersion (MAD) data sets were collected at the European Synchrotron Radiation Facility (ESRF) beamline ID14–4 using an ADSC charge-coupled device (CCD) detector. Two additional crystals were used for data collection at single wavelengths: one at SRS beamline 14.1 using an ADSC CCD, and another at ESRF BM30A using a Mar CCD. Prior to MAD data collection at ID14–4, a fluorescence spectrum for the crystal was obtained, and three data sets were collected at wavelengths corresponding to the fluorescence peak, inflection, and a high energy remote. Table I lists statistics for data collection. We were unable to locate the Se sites using either F_As derived from all three wavelengths or anomalous differences for the peak wavelength only. However, using a highly redundant, lower resolution single anomalous dispersion (SAD) data set collected at SRS 14.1, eight Se sites were readily located using the program SnB (44–46) and subsequently refined with autoSHARP (47). The greater efficiency of determining substructures with high multiplicity SAD data is a common observation (48, 49). The 2.6 Å resolution phases from the SRS 14.1 SAD data set were used to locate Se sites for the 2.3 Å resolution ID14–4 MAD data

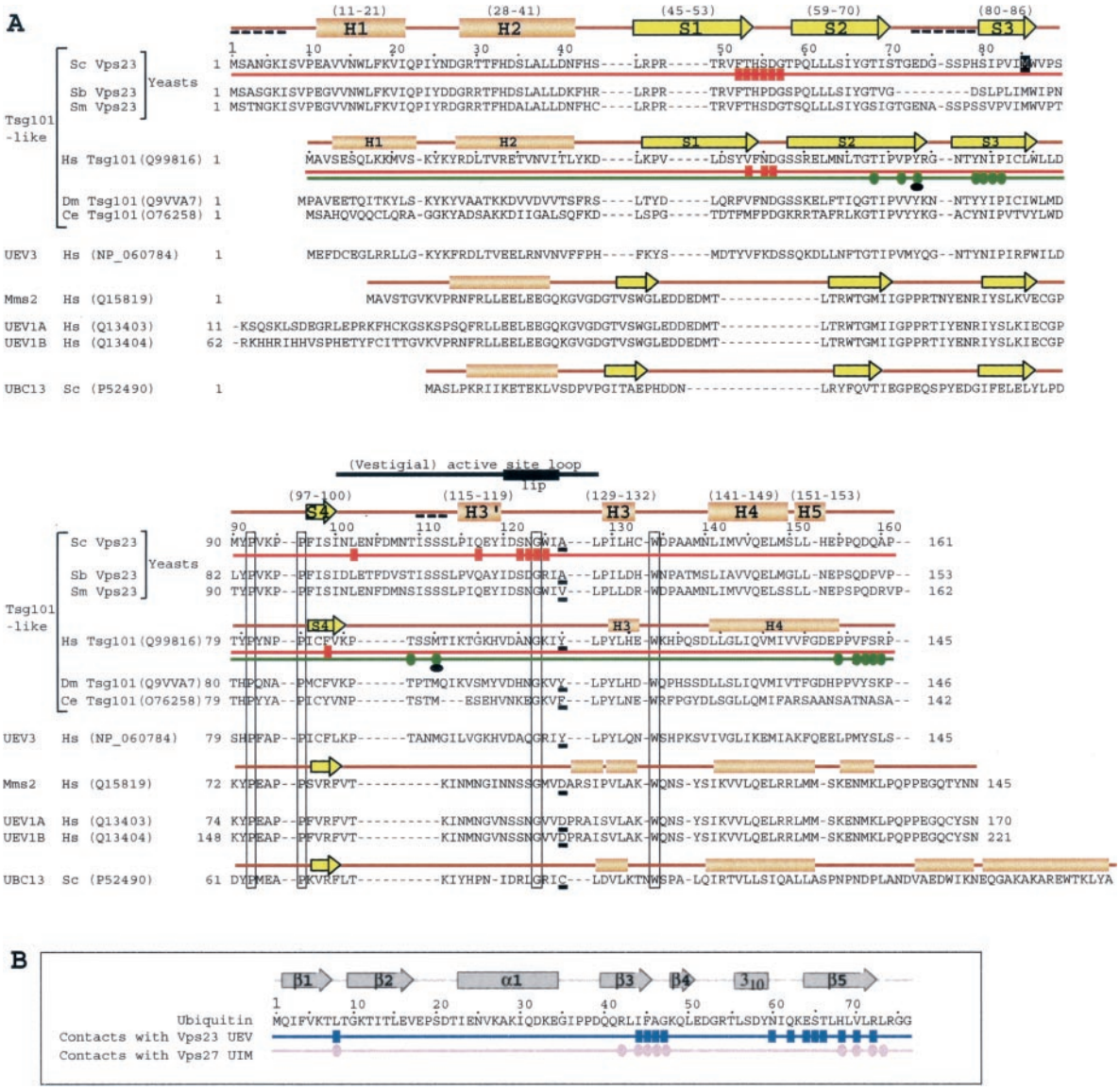

FIG. 2. **Sequence alignment for selected UEV domains and the E2 ligase Ubc13.** *A*, sequence alignments were based on PFAM and manually adjusted to reflect three-dimensional structural alignments where possible. Secondary structure elements are illustrated for the three UEVs having known structures, Vps23, Tsg101, and Mms2, and for Ubc13. *Boxed* residues indicate positions conserved among all UEVs. *Red squares* below the sequence denote residues in contact with Ub in the Vps23/UEV structure and residues in the Tsg101 UEV proposed to interact with Ub on the basis of changes in chemical shifts. Positions marked with *green ovals* identify residues shown to interact with the PTAP peptide in the Tsg101 UEV/PTAP peptide complex. A *black square* marks Met-85$_{Vps23}$ identified by mutagenesis as essential for Vps23 function (12). The Tsg101 residues that were shown by mutagenesis to eliminate p6-PTAP binding *in vitro* or Hrs binding *in vivo* are highlighted by *black ovals* (31, 54). The residue analogous to the catalytic cysteine of the E2 ligases (UBCs) is *underlined*. The vestigial active-site loop is indicated by a *black line*. The *dashed lines* in the secondary structure indicate residues disordered in the Vps23 UEV crystal structure. The species abbreviations are: *Sc*, *S. cerevisiae*; *Sb*, *S. bayanus*; *Sm*, *S. mikatae*; *Hs*, human; *Dm*, *D. melanogaster*; and *Ce*, *C. elegans*. *B*, the sequence and secondary structure of bovine Ub (identical to human Ub). The Ub residues interacting with the Vps23 UEV are marked with *blue squares*, and those interacting with Vps27 UIM-1 (43) are marked with *pink ovals*.

using difference Fourier maps. The 2.3 Å resolution MAD phases were then refined by SHARP (Table I). Solvent flattening was carried out with SOLOMON (50) and DM, using a solvent content of 44% as optimized by SHARP (Fig. 3*A*, *left*). An initial model was built using Arp/warp (51) and refined by alternating rounds of refinement with CNS (52); manual rebuilding was carried out with the program O (53). A final 1.85 Å resolution data set was collected for a Se-Met substituted crystal at ESRF BM30A (Fig. 3*A*, *right*). Final statistics for the 1.85 Å resolution model are given in Table I. There are no residues in the disallowed regions of the Ramachandran plot, and 92% of residues are in the most favored regions, as defined by PROCHECK. Residues 1–7, 73–79, and 110–113 of the UEV are not visible in the electron density for the UEV domain, and the C-terminal residues 75–76 are not visible for the bound ubiquitin.

RESULTS AND DISCUSSION

Structure of the Vps23 UEV Domain—The Vps23 UEV domain was crystallized with Ub in a $P2_12_12_1$ unit cell with dimensions $a = 58.9$, $b = 66.0$, and $c = 69.3$. The asymmetric unit of the crystal contains one Ub and one UEV domain. The UEV fold consists of a twisted four-stranded antiparallel β-sheet having a meander topology, with four α-helices packed against one face of the sheet (Fig. 3*B*). The Vps23 UEV domain has greatly extended and twisted S1 and S2 strands (Fig. 3, *B* and *C*) to form a feature that has been referred to as the β-hairpin "tongue" (54). Our crystal structure of the Vps23 UEV/Ub complex suggests that this feature is important for Ub

TABLE I
Data collection, structure determination, and refinement statistics

MAD data collection and phasing statistics.

	Peak[a]	Inflection[a]	Remote[a]
Data set			
Resolution (Å)	2.3	2.3	2.3
Completeness (last shell)	100.0 (100.0)	100.0 (98.8)	99.9 (100.0)
R_{merge}[b] (last shell)	0.114 (0.197)	0.088 (0.186)	0.085 (0.259)
Redundancy (last shell)	6.3 (4.2)	5.4 (3.6)	5.9 (3.6)
$\langle I/\sigma \rangle$ (last shell)	15.2 (2.87)	15.7 (3.11)	15.9 (2.36)
Phasing statistics			
Phasing power (iso)[c]	0.3		1.08
Phasing power (anom)[c]	1.08	0.78	0.7
Se sites found/expected	8/9		
FOM after SHARP	0.29		
FOM after SOLOMON	0.67		
FOM after DM	0.84		
Medium resolution SAD data collection statistics[d]			
Resolution (Å)	2.6		
Completeness (last shell)	100.0 (100.0)		
R_{merge}[b] (last shell)	0.07 (0.38)		
Redundancy (last shell)	11.4 (11.7)		
$\langle I/\sigma \rangle$ (last shell)	30.1 (4.97)		
High resolution data collection statistics[e]			
Resolution (Å)	1.85		
Completeness (last shell)	99.3 (97.2)		
R_{merge}[b] (last shell)	0.064 (0.37)		
Redundancy (last shell)	9.1 (3.7)		
$\langle I/\sigma \rangle$ (last shell)	22.7 (2.36)		
Refinement statistics			
Resolution (Å) (Number of reflections)		67.0–1.85	(43,667, no cutoff)
Protein atoms		1717	
Waters		126	
R_{cryst}[f]		0.24	
R_{free}[f] (% data used)		0.27 (5.0)	
Root-mean-square deviation from ideality[g] bonds/angles/dihedrals		0.010 Å/1.6°/24.5°	
Average B			
Wilson B factor (Å^2)		30.4 (25.2)	
Root-mean-square deviation B for bonded main (side) chain atoms		1.87 (2.84)	

[a] Data sets were collected at ESRF beamline ID14–4 at 12.6613 keV, 12.6591 keV, and 13.2 keV for the peak, inflection, and remote data sets, respectively.
[b] $R_{merge} = \Sigma_{hkl}\Sigma_i |I_i(hkl) - \langle I(hkl)\rangle|/\Sigma_{hkl}\Sigma_i I_i(hkl)$.
[c] The phasing power is defined as the ratio of the root-mean-square value of the heavy atom structure factor amplitudes to the root-mean-square value of the lack-of-closure error.
[d] Data set was collected at SRS beamline 14.1 at 12.686 keV.
[e] Data set was collected at ESRF beamline BM30A (FIP) at 12.6886 keV.
[f] R_{cryst} and $R_{free} = \Sigma|F_{obs} - F_{calc}| / \Sigma F_{obs}$; R_{free} calculated with the percentage of the data shown in parentheses.
[g] Root-mean-square deviations for bond angles and lengths in regard to Engh and Huber parameters.

binding. Almost all of the intermolecular contacts within the crystal are between the UEV and the Ub. Because of crystal packing, the UEV also contacts a symmetry-related Ub in the vicinity of the PTAP-binding groove (see below), but this contact is unlikely to be functionally significant because it would be mutually exclusive of PTAP-peptide binding; it has been demonstrated that the Tsg101 UEV can bind a PTAP peptide and ubiquitin simultaneously (25, 54). Equilibrium sedimentation analysis indicates that Vps23 UEV is monomeric in solution (see "Experimental Procedures").

Ubiquitin Is Grasped between the β-Hairpin Tongue and the "Lip"—The most extensive contacts between the Ub and the Vps23 UEV involve primarily two loops of the UEV, the β-hairpin tongue and the lip. The S1 and S2 strands of the Vps23 UEV twist around each other at the tip of the β-hairpin tongue so that strand S1 and the S1-S2 loop grasp one end of the Ub, whereas a loop that we will refer to as the lip (residues 120_{Vps23}–126_{Vps23}, flanked by the short helices H3′ and H3 in the vestigial active-site loop) grasps the other end of the Ub molecule. This Ub-binding site comprises the most extensive interactions with Ub in the crystal structure. The Vps23 UEV/Ub interface buries a total surface area of 1319 Å^2. The β-hairpin tongue and the lip contribute 67% of the interface, and almost all of the remainder of the interacting surface derives from other residues in the region between S4 and H3 (known as the vestigial active-site loop, see below). Most of the direct interactions between the UEV and the Ub are Van der Waals interactions (Fig. 4). There are only four direct hydrogen bonds between the UEV and the Ub, and nearly all of these are UEV backbone to Ub side chain interactions. The only UEV side chain forming a hydrogen bond with Ub is Asn-123_{Vps23} at the tip of the lip, which interacts with Thr-66_{Ub}. Much of the interface is composed of backbone atoms or small residues. The tip of the β-hairpin tongue (52_{Vps23}–59_{Vps23}) has either small residues or larger residues, such as the strictly conserved Asp-56_{Vps23}, with side chains directed away from the bound Ub, so that this structural element makes many Van der Waals contacts using its backbone atoms (Fig. 4). This role of UEV backbone atoms involved in contacts with Ub is also seen in the lip. The tip of the lip contacts the N-terminal end of Ub strand β5, whereas backbone atoms from the Ub β3/β4 turn (Ala-46_{Ub} and Gly-47_{Ub}) slot between the β-hairpin tongue and the lip to rest on a hydrophobic platform formed by the side chains of residues Trp-125_{Vps23} and Phe-52_{Vps23} (Fig. 4). Interactions of the Ub β3/β4 loop with the C-terminal half of the lip include the completely conserved Gly-124_{Vps23}. There are several water-mediated interactions at the interface, including six waters that make direct interactions with both the Vps23 and the bound Ub. The abundance of weak Van der Waals and water-mediated interactions in the interface is consistent with the

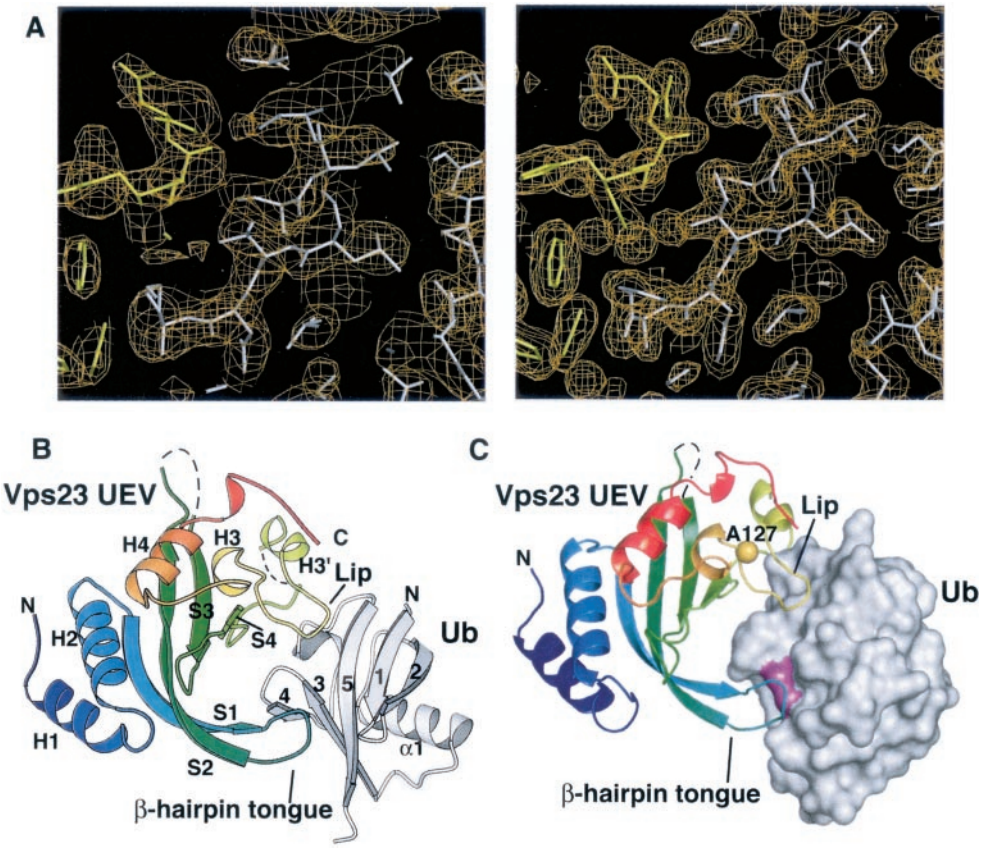

FIG. 3. **The structure of the Vps23 UEV/Ub complex.** *A*, an illustration of the 2.3 Å electron density map calculated with MAD phases after solvent flattening with SOLOMON with the initial model (*left*); the 1.85 Å resolution mFo-DFc difference electron density map, and the final model after refinement calculated with data from the higher resolution crystal (*right*) (see Table I). The maps illustrate a slab from the UEV (*yellow*)/Ub (*white*) interface. *B*, the ribbon diagram of the Vps23 UEV domain is colored in rainbow colors from *blue* (N terminus) to *red* (C terminus). The bound ubiquitin (*Ub*) is shown in *gray*. *C*, the Ub is shown in solid representation with Ile-44, which is located at the center of the UEV-interacting surface and is essential for endocytosis, highlighted in *purple*. The Vps23 UEV is colored as in *B*. Ala-127 (*A127*), analogous to the catalytic cysteine of the E2 ligases, is represented as an *orange sphere*.

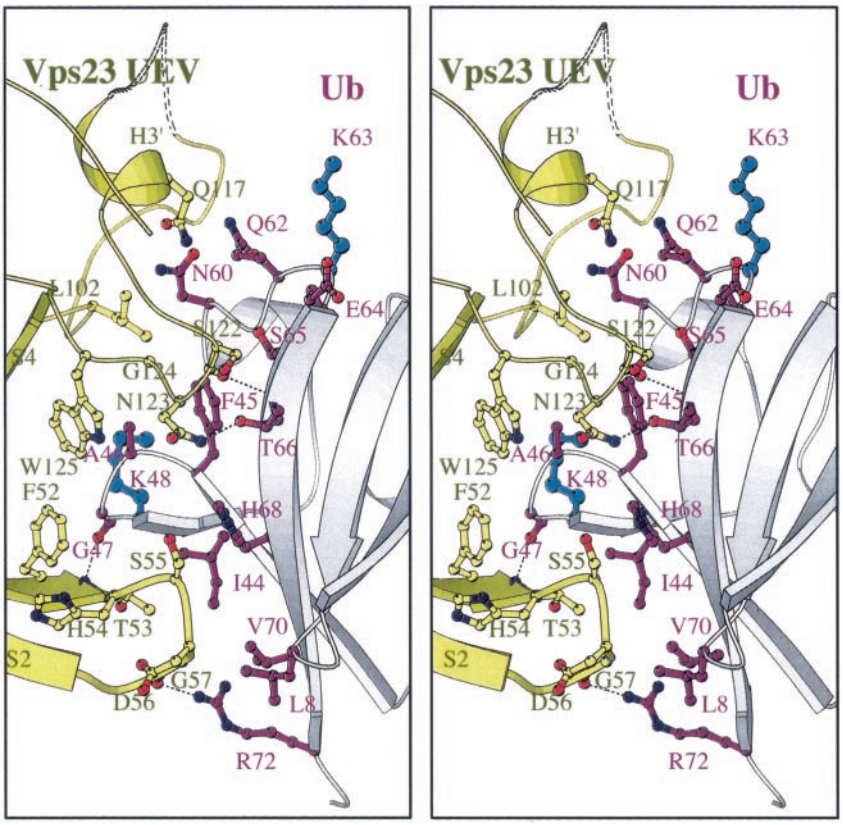

FIG. 4. **Stereo representation of the detailed interactions between the UEV and the bound Ub.** Residues in direct contact (closer than 4.0 Å) between the Vps23 UEV (*yellow*) and the Ub (*magenta*) are labeled. Direct hydrogen bonds between the UEV and the Ub are indicated as *dashed lines*.

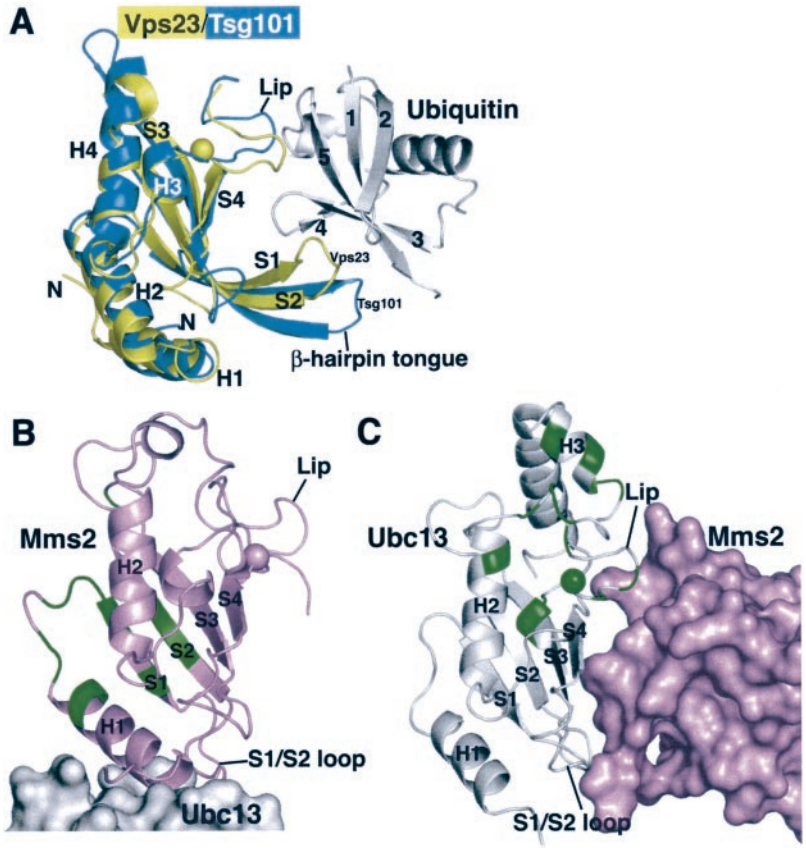

FIG. 5. **A comparison of the three structurally characterized UEV domains.** *A*, the Vps23 UEV (*yellow*) is superimposed on the Tsg101 UEV (*cyan*). The Ub bound in the Vps23 UEV/Ub complex is colored *gray*. Part of the vestigial active-site loop (S4/lip loop) has been omitted for clarity. *B*, the human Ubc13 (*gray molecular surface*)/Mms2 (*magenta ribbon*) heterodimer with the Mms2 oriented as the UEV in *A*. Residues showing the greatest chemical shift changes upon addition of Ub are highlighted in *green* (68). *C*, the Mms2 (*magenta molecular surface*)/Ubc13 (*gray ribbon*) heterodimer with the Ubc13 oriented as in *A*. Residues showing the greatest chemical shift changes upon formation of the Ub thiolester are highlighted in *green* (68). The residue analogous to the catalytic cysteine is represented as a *sphere* in each of the three UEV domains.

low affinity (>500 μM) of the Tsg101 UEV/Ub interaction measured in solution (25, 54). The importance of the β-hairpin tongue in interactions with the bound Ub is consistent with the NMR chemical shift changes reported for the Tsg101 UEV upon Ub binding and with the effects of site-specific mutagenesis (54).

Both Unique and Commonly Exploited Ub Surfaces Interact with the ESCRT-I UEV—Ubiquitin presents two adjacent patches for interaction with the Vps23 UEV. One of the patches is a largely hydrophobic Leu-8_{Ub}/Ile-44_{Ub}/Val-70_{Ub} patch, which makes important contacts with the β-hairpin tongue, whereas the other is a predominately hydrophilic Asn-60_{Ub}/Gln-62_{Ub}/Glu-64_{Ub} patch, which contacts residues in the vestigial active-site loop. Together, these patches represent the most extensive UEV/Ub interaction in the crystal and include the loops $\beta1_{Ub}/\beta2_{Ub}$, $\beta3_{Ub}/\beta4_{Ub}$, and $\beta4_{Ub}/\beta5_{Ub}$ and residues from strands $\beta3_{Ub}$ and $\beta5_{Ub}$ (Fig. 2*B*). Consistent with our structure, a recent report showed that mutations of Ub residues in either of these patches reduce binding to the Vps23 UEV (29). Interestingly, no single point mutation of Ub had a measurable effect upon Vps23 UEV binding. However, double mutants in either the hydrophobic patch (L8A/V70A) or the hydrophilic patch (Q62A/E64A) reduced binding to Vps23 UEV. A complete loss of binding was observed when mutations in the hydrophilic patch were combined with a hydrophobic patch mutation (Q62A/E64A/I44A) (29). All of the Ub residues whose mutation reduced binding to Vps23 UEV are in contact with the Vps23 UEV in our crystal structure (residues 8_{Ub}, 44_{Ub}, 62_{Ub}, 64_{Ub}, 70_{Ub}).

The Leu-8_{Ub}/Ile-44_{Ub}/Val-70_{Ub} hydrophobic patch is important both in endocytosis of mono-ubiquitinated proteins and proteasomal degradation of polyubiquitinated proteins (55). Ub Ile-44_{Ub}, which is near the center of the hydrophobic surface patch, and residues near it are important for interactions with Ub-binding modules NZF, CUE, UBA, and UIM (34–41, 43). Although the hydrophobic patch interacts with many Ub-binding domains, including those of Vps27 (43), it appears that the hydrophilic patch of Ub encompasses residues forming interactions specific for ESCRT-I UEV relative to Vps27 (Fig. 2*B*), because the Q62A/E64A double mutation did not affect Vps27 binding (29).

Lys-48_{Ub} of the Ub bound to Vps23 UEV has a greatly restricted access, suggesting that the Vps23 UEV might prevent the covalent addition of another Ub to Lys-48_{Ub} of the ubiquitinated cargo. However, restricted access of Lys-48_{Ub} is not a signature of mono-ubiquitin recognition because the Vps27 UIMs also recognize mono-ubiquitinated cargo, but the structure of the Vps27 UIM/Ub complex showed that Lys-48_{Ub} is well exposed to solvent (43). In contrast to Lys-48_{Ub}, Lys-63_{Ub} is fully exposed in both the Vps23 UEV/Ub and Vps27 UIM/Ub complexes. This may be related to the observation that Lys-63_{Ub} polyubiquitination stimulates endocytosis of yeast uracil permease (10).

The UEV Domains Share a Common Fold but Use This Fold to Make Diverse Interactions—The structure of the Vps23 UEV domain has an overall fold that is similar to the two other structurally characterized UEV domains, human Tsg101 (54) and Mms2 (56, 57) (Fig. 5, *A* and *B*). Furthermore, the UEV domains have a core structure that agrees closely with the E2 Ub-conjugating enzymes (UBC) (Fig. 5*C*; Refs. 54, 58–64). However, there are two prominent differences between the Vps23 and Tsg101 UEV domains and either the Mms2 UEV or Ubc13. Both the Tsg101 UEV (54) and the Vps23 UEV have strands S1 and S2 extended into a β-hairpin tongue, and both have an additional N-terminal helix. These features are critical to molecular recognition by the UEVs. The β-hairpin tongue is central to the unique interactions that the Vps23 UEV makes with Ub. Consequently, it is not surprising that the structure of this loop is unique for the ESCRT-I UEVs as compared with other UEVs and E2 ligases. The S1-S2 loop in the Mms2 does

not form an extended β-hairpin tongue. Instead, this region forms a squat loop that projects nearly perpendicularly to the direction of the S1 and S2 strands and away from the core of the Mms2 UEV to interact with E2 Ub-conjugating enzyme Ubc13 (Fig. 5*B*; Refs. 56, 57). Similarly, the S1-S2 loop of Ubc13 interacts with Mms2, and the bound Mms2 covers a surface of Ubc13 analogous to the Vps23 UEV surface interacting with Ub (Fig. 5*C*). The additional N-terminal helix of the Vps23/Tsg101 UEVs lays against the core structure in a location analogous to the region in Mms2 that interacts with the Ubc13 (Fig. 5, *A* and *B*). Consequently, Vps23/Tsg101 UEVs cannot act as partners of Ubc13.

Binding Ub Seems to Induce Conformational Changes in the UEV Tongue and Lip—Relative to the Tsg101 UEV structure determined in the absence of Ub (54), both the β-hairpin tongue and the lip move toward each other to engage the bound Ub in a pincer-like fashion (Fig. 5*A*). The large differences in the relative positions of the β-hairpin tongue and the lip in the Vps23 UEV/Ub complex in comparison to the Tsg101 UEV in the absence of Ub suggest that there are conformational changes induced by Ub binding (Fig. 5*A*). Consistent with this suggestion, there are residues showing large Ub-induced chemical shift changes in Tsg101, *e.g.* residue Trp-75_{Tsg101} (equivalent of Trp-86_{Vps23}), which both mutational analysis (54) and our structure indicate are not involved in direct Ub interaction.

Among the UEVs, the Vestigial Active-site Loop Assumes Diverse Functions and Conformations—The region between strand S4 and helix H3 has been referred to as the "vestigial active-site loop" because it is analogous with the region containing the active-site cysteine in the E2 ligases. This loop, which is highly variable in sequence among the UEVs and E2 ligases, forms pivotal interactions with Ub and much of the PTAP interaction with the Tsg101 UEV (65). The lip is a loop in the C-terminal half of the vestigial active-site loop and it constitutes a distinct structural element common to the E2 ligases and the UEVs (Fig. 5). Ala-127_{Vps23} at the base of the lip is homologous to the conserved catalytic cysteine residue in the active site of the E2 ligases (Fig. 5).

Although the Tsg101/Vps23 UEV has no catalytic activity, the lip region has a conformation that fairly closely agrees with the E2 ligases (Fig. 5). However, in the Vps23 UEV/Ub complex compared with the Tsg101 UEV, the lip is displaced by a hinge-type motion around two hydrophobic residues (Ile-120_{Vps23} and Ile-126_{Vps23}) that anchor the base of the loop into the core of the domain (Figs. 5*A* and 6). This hinge motion brings the Vps23 UEV lip into contact with ubiquitin. The apparent hinge motion of the lip of the Vps23 UEV compared with Tsg101 is likely because of the presence of the bound Ub because the lip region of these two proteins shows relatively little sequence variation. The role for the Vps23 lip of the vestigial active-site loop in Ub recognition is likely to be conserved in Tsg101 because some chemical shift changes were observed in the Tsg101 vestigial active-site loop. Although no specific residues involved in this interaction were identified in the NMR study (54), site-specific mutagenesis of Phe-88_{Tsg101} just preceding the vestigial active-site loop was shown to greatly decrease the affinity for Ub. The Vps23 residue whose backbone position most nearly superimposes on Phe-88_{Tsg101}, Ser-99_{Vps23}, is not involved in Ub binding; however, the bulky side chain of the lip residue Trp-125_{Vps23} occupies the space analogous to that occupied by the Phe-88_{Tsg101} side chain, and Trp-125_{Vps23} forms key interactions with Ub (Fig. 4). In addition to its likely role in interacting with Ub, the lip of the Tsg101 UEV also has a role in supporting the N-terminal part of the vestigial active-site loop (referred to as the S4/lip loop) that is critical for PTAP-motif binding. The hinge angle of the

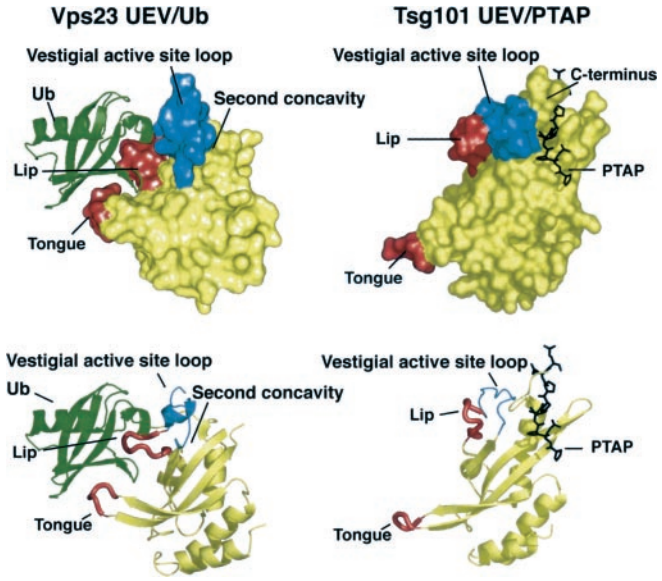

FIG. 6. **A comparison of the yeast and human ESCRT-I UEVs.** *Left*, representations of the Vps23 UEV/Ub complex; *right*, representations of the Tsg101 UEV complex with a PTAP-peptide from the HIV-1 p6 protein (65). The vestigial active-site loop is colored *cyan* and the β-hairpin tongue and lip are colored *red*. The Ub bound to the Vps23 UEV is colored *green*, and the PTAP peptide bound to Tsg101 is colored *black*.

lip of the E2 ligase Ubc13 is very similar to that of the Tsg101 UEV lip (Fig. 5). However, the function of the lip in the E2 ligases and the UEVs is quite different. In the Ubc13, the tip of the lip interacts with the Mms2 UEV in the Ubc13/Mms2 heterodimer (Fig. 5*C*).

Two Distinct UEV Surfaces Accommodate Ub and Hrs/Vps27—The vestigial active-site loop bisects the concave surface of the UEV β-sheet. On either side of this loop, the surface of the β-sheet curves away to present two exposed, concave surfaces (Fig. 6). One concavity contains Ub, which interacts with the β-hairpin tongue and one face of the vestigial active-site loop (the lip in particular). The second concavity bordered by the opposite face of the vestigial active-site loop is broadly analogous to the PTAP-binding groove of the Tsg101 UEV (Fig. 6). The P(T/S)AP-like motifs are present in adaptor proteins Vps27 and Hrs and are used for direct interactions with Vps23 and Tsg101 UEVs, respectively. The Vps23 UEV interacts with PSDP and PTVP sequence motifs in Vps27 (28, 29), whereas the Tsg101 UEV interacts with the PSAP motif of Hrs (and the PTAP motif present in the HIV-1 p6 protein) (30–32). Therefore, it is likely that this second concavity of the Vps23 UEV accommodates a PSDP or PTVP motif in a manner analogous to the Tsg101/P(S/T)AP interaction. The great sequence divergence in the N-terminal half of the vestigial active-site loop between the Vps23 and Tsg101 UEVs (including a six residue insertion in Vps23 relative to Tsg101) might explain their binding to related, but distinct P*XX*P motifs.

CONCLUSIONS

The structure of the complex between the Vps23 UEV and Ub shows clearly the detailed interactions that lead to specific Ub recognition. Two structural elements from the Vps23 UEV, the extended β-hairpin tongue and the vestigial active-site loop, comprise a bipartite interaction with the Ub. Although the β-hairpin tongue contacts a hydrophobic patch on the surface of the Ub that is involved in interaction with a broad range of Ub-interacting domains, including the Vps27 UIM domains, the ESCRT-I UEVs also contact a predominately hydrophilic Ub patch that is not involved in the Vps27/Ub interactions (Fig.

2*B*). The partial overlap of the Vps27 and Vps23 interactions with the hydrophobic patch on the Ub indicates that these proteins cannot simultaneously interact with the same Ub moiety. This suggests a sequential model in which Vps27 initially engages ubiquitinated cargo, localizing it within flat clathrin-coated patches on the endosomal surface (reviewed in Ref. 66), and then the ubiquitinated cargo is passed to ESCRT-I prior to the inward budding of the limiting endosomal membrane to generate MVBs. The structure provides a clear view of the distinct surfaces on both the ESCRT-I UEVs and Ub that can be targeted for specific disruption of either Vps23/Tsg101- or Vps27/Hrs-dependent steps in ubiquitinated cargo sorting. Further structural insights into the interactions of Ub with a range of Ub-recognition modules may facilitate the design of Ub mutants affecting other specific Ub-dependent pathways. Structural studies of the intact ESCRT-I complex with ubiquitinated cargo will shed more light on the mechanism whereby this complex assists in sorting cargo into MVBs.

Acknowledgments—We thank Mark Allen for collecting the SRS 14.1 data set, Joanne McCarthy for assistance with data collection at ESRF beamline ID14–4, Michel Pirrochi for assistance with data collection at ESRF FIP beamline BM30A, and Mike MacDonald for assistance at SRS 14.1. We thank Olga Perisic for critical reading of the manuscript.

REFERENCES

1. Chau, V., Tobias, J. W., Bachmair, A., Marriott, D., Ecker, D. J., Gonda, D. K., and Varshavsky, A. (1989) *Science* **243,** 1576–1583
2. Thrower, J. S., Hoffman, L., Rechsteiner, M., and Pickart, C. M. (2000) *EMBO J.* **19,** 94–102
3. Bonifacino, J. S., and Traub, L. M. (2003) *Annu. Rev. Biochem.* **72,** 395–447
4. Raiborg, C., Rusten, T. E., and Stenmark, H. (2003) *Curr. Opin. Cell Biol.* **15,** 446–455
5. Katzmann, D. J., Odorizzi, G., and Emr, S. D. (2002) *Nat. Rev. Mol. Cell. Biol.* **3,** 893–905
6. Hicke, L., and Dunn, R. (2003) *Annu. Rev. Cell Dev. Biol.* **19,** 141–172
7. Peschard, P., and Park, M. (2003) *Cancer Cell* **3,** 519–523
8. Haglund, K., Sigismund, S., Polo, S., Szymkiewicz, I., Di Fiore, P. P., and Dikic, I. (2003) *Nat. Cell. Bio.* **5,** 461–466
9. Mosesson, Y., Shtiegman, K., Katz, M., Zwang, Y., Vereb, G., Szollosi, J., and Yarden, Y. (2003) *J. Biol. Chem.* **278,** 21323–21326
10. Galan, J.-M., and Haguenauer-Tsapis, R. (1997) *EMBO J.* **16,** 5847–5854
11. Piper, R. C., and Luzio, J. P. (2001) *Traffic* **2,** 612–621
12. Katzmann, D. J., Babst, M., and Emr, S. D. (2001) *Cell* **106,** 145–155
13. Babst, M., Odorizzi, G., Estepa, E. J., and Emr, S. D. (2000) *Traffic* **1,** 248–258
14. Bishop, N., and Woodman, P. (2001) *J. Biol. Chem.* **276,** 11735–11742
15. Ponting, C. P., Cai, Y. D., and Bork, P. (1997) *J. Mol. Med.* **75,** 467–469
16. Koonin, E. V., and Abagyan, R. A. (1997) *Nat. Genet.* **16,** 330–331
17. Sancho, E., Vila, M. R., Sanchez-Pulido, L., Lozano, J. J., Paciucci, R., Nadal, M., Fox, M., Harvey, C., Bercovich, B., Loukili, N., Ciechanover, A., Lin, S. L., Sanz, F., Estivill, X., Valencia, A., and Thomson, T. M. (1998) *Mol. Cell. Biol.* **18,** 576–589
18. Villalobo, E., Morin, L., Moch, C., Lescasse, R., Hanna, M., Xiao, W., and Baroin-Tourancheau, A. (2002) *Mol. Biol. Evol.* **19,** 39–48
19. Hofmann, R. M., and Pickart, C. M. (1999) *Cell* **96,** 645–653
20. Deng, L., Wang, C., Spencer, E., Yang, L., Braun, A., You, J., Slaughter, C., Pickart, C., and Chen, Z. J. (2000) *Cell* **103,** 351–361
21. Hoege, C., Pfander, B., Moldovan, G. L., Pyrowolakis, G., and Jentsch, S. (2002) *Nature* **419,** 135–141
22. Thomson, T. M., Lozano, J. J., Loukili, N., Carrio, R., Serras, F., Cormand, B., Valeri, M., Diaz, V. M., Abril, J., Burset, M., Merino, J., Macaya, A., Corominas, M., and Guigo, R. (2000) *Genome Res.* **10,** 1743–1756
23. Kloor, M., Bork, P., Duwe, A., Klaes, R., von Knebel Doeberitz, M., and Ridder, R. (2002) *Biochim. Biophys. Acta* **1579,** 219–224
24. Bishop, N., Horman, A., and Woodman, P. (2002) *J. Cell Biol.* **157,** 91–102
25. Garrus, J. E., von Schwedler, U. K., Pornillos, O. W., Morham, S. G., Zavitz, K. H., Wang, H. E., Wettstein, D. A., Stray, K. M., Cote, M., Rich, R. L., Myszka, D. G., and Sundquist, W. I. (2001) *Cell* **107,** 55–65
26. Martin-Serrano, J., Zang, T., and Bieniasz, P. D. (2001) *Nat. Med.* **7,** 1313–1319
27. VerPlank, L., Bouamr, F., LaGrassa, T. J., Agresta, B., Kikonyogo, A., Leis, J., and Carter, C. A. (2001) *Proc. Natl. Acad. Sci. U. S. A.* **98,** 7724–7729
28. Katzmann, D. J., Stefan, C. J., Babst, M., and Emr, S. D. (2003) *J. Cell Biol.* **162,** 413–423
29. Bilodeau, P. S., Winistorfer, S. C., Kearney, W. R., Robertson, A. D., and Piper, R. C. (2003) *J. Cell Biol.* **163,** 237–243
30. Lu, Q., Hope, L. W., Brasch, M., Reinhard, C., and Cohen, S. N. (2003) *Proc. Natl. Acad. Sci. U. S. A.* **100,** 7626–7631
31. Pornillos, O., Higginson, D. S., Stray, K. M., Fisher, R. D., Garrus, J. E., Payne, M., He, G.-P., Wang, H. E., Morham, S. G., and Sundquist, W. I. (2003) *J. Cell Biol.* **162,** 425–434
32. Bache, K. G., Brech, A., Mehlum, A., and Stenmark, H. (2003) *J. Cell Biol.* **162,** 435–442
33. Martin-Serrano, J., Zang, T., and Bieniasz, P. D. (2003) *J. Virol.* **77,** 4794–4804
34. Wang, B., Alam, S. L., Meyer, H. H., Payne, M., Stemmler, T. L., Davis, D. R., and Sundquist, W. I. (2003) *J. Biol. Chem.* **278,** 20225–20234
35. Prag, G., Misra, S., Jones, E. A., Ghirlando, R., Davies, B. A., Horazdovsky, B. F., and Hurley, J. H. (2003) *Cell* **113,** 609–620
36. Kang, R. S., Daniels, C. M., Francis, S. A., Shih, S. C., Salerno, W. J., Hicke, L., and Radhakrishnan, I. (2003) *Cell* **113,** 621–630
37. Shih, S. C., Prag, G., Francis, S. A., Sutanto, M. A., Hurley, J. H., and Hicke, L. (2003) *EMBO J.* **22,** 1273–1281
38. Ciani, B., Layfield, R., Cavey, J. R., Sheppard, P. W., and Searle, M. S. (2003) *J. Biol. Chem.* **278,** 37409–37412
39. Ryu, K. S., Lee, K. J., Bae, S. H., Kim, B. K., Kim, K. A., and Choi, B. S. (2003) *J. Biol. Chem.* **278,** 36621–36627
40. Mueller, T. D., and Feigon, J. (2002) *J. Mol. Biol.* **319,** 1243–1255
41. Fisher, R. D., Wang, B., Alam, S. L., Higginson, D. S., Robinson, H., Sundquist, W. I., and Hill, C. P. (2003) *J. Biol. Chem.* **278,** 28976–28984
42. Hook, S. S., Orian, A., Cowley, S. M., and Eisenman, R. N. (2002) *Proc. Natl. Acad. Sci. U. S. A.* **99,** 13425–13430
43. Swanson, K. A., Kang, R. S., Stamenova, S. D., Hicke, L., and Radhakrishnan, I. (2003) *EMBO J.* **22,** 4597–4606
44. Weeks, C. M., and Miller, R. (1999) *J. Appl. Crystallogr.* **32,** 120–124
45. Smith, G. D., Nagar, B., Rini, J. M., Hauptman, H. A., and Blessing, R. H. (1998) *Acta Crystallogr. Sec. D* **54,** 799–804
46. Turner, M. A., Yuan, C.-S., Borchardt, R. T., Hershfield, M. S., Smith, G. D., and Howell, L. L. (1998) *Nat. Struct. Biol.* **5,** 369–376
47. de La Fortelle, E., and Bricogne, G. (1997) *Methods Enzymol.* **276,** 472–494
48. Howell, P. L., Blessing, R. H., Smith, G. D., and Weeks, C. M. (2000) *Acta Crystallogr. Sec. D* **56,** 604–617
49. Uson, I., Schmidt, B., von Bulow, R., Grimme, S., von Figura, K., Dauter, M., Rajashankar, K. R., Dauter, Z., and Sheldrick, G. M. (2003) *Acta Crystallogr. Sec. D* **59,** 57–66
50. Abrahams, J. P., and Leslie, A. G. W. (1996) *Acta Crystallogr. Sec. D* **52,** 30–42
51. Perrakis, A., Morris, R., and Lamzin, V. S. (1999) *Nat. Struct. Biol.* **6,** 458–463
52. Brünger, A. T., Adams, P. D., Clore, G. M., DeLano, W. L., Gros, P., Grosse-Kunstleve, R. W., Jiang, J. S., Kuszewski, J., Nilges, M., Pannu, N. S., Read, R. J., Rice, L. M., Simonson, T., and Warren, G. L. (1998) *Acta Crystallogr. Sec. D* **54,** 905–921
53. Jones, T. A., Zou, J.-Y., Cowan, S. W., and Kjeldgaard, M. (1991) *Acta Crystallogr. Sec. A* **47,** 110–119
54. Pornillos, O., Alam, S. L., Rich, R. L., Myszka, D. G., Davis, D. R., and Sundquist, W. I. (2002) *EMBO J.* **21,** 2397–2406
55. Sloper-Mould, K. E., Jemc, J. C., Pickart, C. M., and Hicke, L. (2001) *J. Biol. Chem.* **276,** 30483–30489
56. VanDemark, A. P., Hofmann, R. M., Tsui, C., Pickart, C. M., and Wolberger, C. (2001) *Cell* **105,** 711–720
57. Moraes, T. F., Edwards, R. A., McKenna, S., Pastushok, L., Xiao, W., Glover, J. N., and Ellison, M. J. (2001) *Nat. Struct. Biol.* **8,** 669–673
58. Cook, W. J., Jeffrey, L. C., Xu, Y., and Chau, V. (1993) *Biochemistry* **32,** 13809–13817
59. Cook, W. J., Martin, P. D., Edwards, B. F., Yamazaki, R. K., and Chau, V. (1997) *Biochemistry* **36,** 1621–1627
60. Tong, H., Hateboer, G., Perrakis, A., Bernards, R., and Sixma, T. K. (1997) *J. Biol. Chem.* **272,** 21381–21387
61. Worthylake, D. K., Prakash, S., Prakash, L., and Hill, C. P. (1998) *J. Biol. Chem.* **273,** 6271–6276
62. Joazeiro, C. A., Wing, S. S., Huang, H., Leverson, J. D., Hunter, T., and Liu, Y. C. (1999) *Science* **286,** 309–312
63. Jiang, F., and Basavappa, R. (1999) *Biochemistry* **38,** 6471–6478
64. Hamilton, K. S., Ellison, M. J., Barber, K. R., Williams, R. S., Huzil, J. T., McKenna, S., Ptak, C., Glover, M., and Shaw, G. S. (2001) *Structure* **9,** 897–904
65. Pornillos, O., Alam, S. L., Davis, D. R., and Sundquist, W. I. (2002) *Nat. Struct. Biol.* **9,** 812–817
66. Clague, M. J., and Urbe, S. (2003) *Trends Cell Biol.* **13,** 603–606
67. Feng, G. H., Lih, C. J., and Cohen, S. N. (2000) *Cancer Res.* **60,** 1736–1741
68. McKenna, S., Moraes, T., Pastushok, L., Ptak, C., Xiao, W., Spyracopoulos, L., and Ellison, M. J. (2003) *J. Biol. Chem.* **278,** 13151–13158